

Multiple Instance Active Learning for Object Detection

Tianning Yuan[†], Fang Wan^{†*}, Mengying Fu[†],
Jianzhuang Liu[‡], Songcen Xu[‡], Xiangyang Ji[§] and Qixiang Ye^{†*}

[†]University of Chinese Academy of Sciences, Beijing, China

[‡]Noah’s Ark Lab, Huawei Technologies, Shenzhen, China. [§]Tsinghua University, Beijing, China

{yuantianning19, fumengying19}@mails.ucas.ac.cn, {wanfang, qxye}@ucas.ac.cn

{liu.jianzhuang, xusongcen}@huawei.com, xyji@tsinghua.edu.cn

Abstract

Despite the substantial progress of active learning for image recognition, there still lacks an instance-level active learning method specified for object detection. In this paper, we propose Multiple Instance Active Object Detection (MI-AOD), to select the most informative images for detector training by observing instance-level uncertainty. MI-AOD defines an instance uncertainty learning module, which leverages the discrepancy of two adversarial instance classifiers trained on the labeled set to predict instance uncertainty of the unlabeled set. MI-AOD treats unlabeled images as instance bags and feature anchors in images as instances, and estimates the image uncertainty by re-weighting instances in a multiple instance learning (MIL) fashion. Iterative instance uncertainty learning and re-weighting facilitate suppressing noisy instances, toward bridging the gap between instance uncertainty and image-level uncertainty. Experiments validate that MI-AOD sets a solid baseline for instance-level active learning. On commonly used object detection datasets, MI-AOD outperforms state-of-the-art methods with significant margins, particularly when the labeled sets are small. Code is available at <https://github.com/yuantn/MI-AOD>.

1. Introduction

The key idea of active learning is that a machine learning algorithm can achieve better performance with fewer training samples if it is allowed to select which to learn. Despite the rapid progress of the methods with less supervision [21, 20], e.g., weak supervision and semi-supervision,

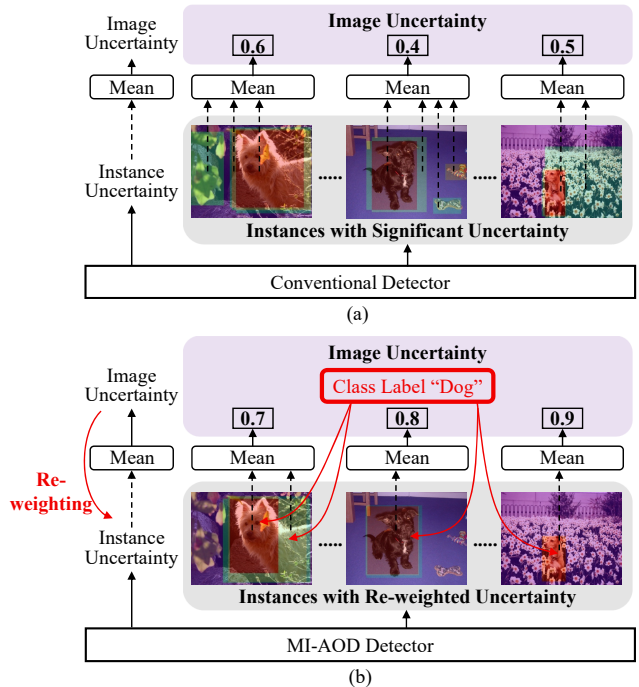


Figure 1. Comparison of active object detection methods. (a) Conventional methods compute image uncertainty by simply averaging instance uncertainties, ignoring interference from a large number of background instances. (b) Our MI-AOD leverages uncertainty re-weighting via multiple instance learning to filter out interfering instances while bridging the gap between instance uncertainty and image uncertainty. (Best viewed in color)

active learning remains the cornerstone of many practical applications for its simplicity and higher performance.

In the computer vision area, active learning has been widely explored for image classification (active image classification) by empirically generalizing the model trained on the labeled set to the unlabeled set [9, 30, 18, 39, 4, 24, 36,

*Corresponding Authors.

[\[25, 34\]](#). Uncertainty-based methods define various metrics for selecting informative images and adapting trained models to the unlabeled set [\[9\]](#). Distribution-based approaches [\[30, 1\]](#) aim at estimating the layout of unlabeled images to select samples of large diversity. Expected model change methods [\[8, 15\]](#) find out samples that can cause the greatest change of model parameters or the largest loss [\[42\]](#).

Despite the substantial progress, there still lacks an instance-level active learning method specified for object detection (*i.e.*, active object detection [\[42, 43, 2\]](#)), where the instance denotes the object proposal in an image. The objective goal of active object detection is to select the most informative images for detector training. However, the recent methods tackled it by simply summarizing/averaging instance/pixel uncertainty as image uncertainty and unfortunately ignored the large imbalance of negative instances in object detection, which causes significant noisy instances in the background and interferes with the learning of image uncertainty, Fig. 1(a). The noisy instances also cause the inconsistency between image and instance uncertainty, which hinders selecting informative images.

In this paper, we propose a Multiple Instance Active Object Detection (MI-AOD) approach, Fig. 1(b), and target at selecting informative images from the unlabeled set by learning and re-weighting instance uncertainty with discrepancy learning and multiple instance learning (MIL). To learn the instance-level uncertainty, MI-AOD first defines an instance uncertainty learning (IUL) module, which leverages two adversarial instance classifiers plugged atop the detection network (*e.g.*, a feature pyramid network) to learn the uncertainty of unlabeled instances. Maximizing the prediction discrepancy of two instance classifiers predicts instance uncertainty while minimizing classifiers' discrepancy drives learning features to reduce the distribution bias between the labeled and unlabeled instances.

To establish the relationship between instance uncertainty and image uncertainty, MI-AOD incorporates a MIL module, which is in parallel with the instance classifiers. MIL treats each unlabeled image as an instance bag and performs instance uncertainty re-weighting (IUR) by evaluating instance appearance consistency across images. During MIL, the instance uncertainty and image uncertainty are forced to be consistently driven by a classification loss defined on image class labels (or pseudo-labels). Optimizing the image-level classification loss facilitates suppressing the noisy instances while highlighting truly representative ones. Iterative instance uncertainty learning and instance uncertainty re-weighting bridge the gap between instance-level observation and image-level evaluation, towards selecting the most informative images for detector training.

The contributions of this paper include:

(1) We propose Multiple Instance Active Object Detection (MI-AOD), establishing a solid baseline to model the

relationship between the instance uncertainty and image uncertainty for informative image selection.

(2) We design instance uncertainty learning (IUL) and instance uncertainty re-weighting (IUR) modules, providing effective approaches to highlight informative instances while filtering out noisy ones in object detection.

(3) We apply MI-AOD to object detection on commonly used datasets, improving state-of-the-art methods with significant margins.

2. Related Work

2.1. Active Learning

Uncertainty-based Methods. Uncertainty is the most popular metric to select samples for active learning [\[31\]](#), which can be defined as the posterior probability of a predicted class [\[17, 16\]](#), or the margin between the posterior probabilities of the first and the second predicted class [\[14, 28\]](#). It can also be defined upon entropy [\[32, 26, 14\]](#) to measure the variance of unlabeled samples. The expected model change methods [\[29, 33\]](#) utilized the present model to estimate the expected gradient or prediction changes [\[8, 15\]](#) for sample selection. MIL-based methods [\[33, 13, 40, 6\]](#) selected informative images by discovering representative instances. However, they are designed for image classification and not applicable to object detection due to the challenging aspect of crowded and noisy instances [\[38, 37\]](#).

Distribution-based Methods. These methods select diverse samples by estimating the distribution of unlabeled samples. Clusters [\[27\]](#) were applied to build the unlabeled sample distribution while discrete optimization methods [\[11, 7, 41\]](#) were employed to perform sample selection. Considering the distances to the surrounding samples, the context-aware methods [\[12, 3\]](#) selected the samples that can represent the global sample distribution. Core-set [\[30\]](#) defined active learning as core-set selection, *i.e.*, choosing a set of points such that a model learned on the labeled set can capture the diversity of the unlabeled samples.

In the deep learning era, active learning methods remain falling into the uncertainty-based or distribution-based routines [\[18, 39, 4\]](#). Sophisticated methods extended active learning to the open sets [\[24\]](#), or combined it with self-paced learning [\[36\]](#). Nevertheless, it remains questionable whether the intermediate feature representation is effective for sample selection. The learning loss method [\[42\]](#) can be categorized as either uncertainty-based or distribution-based. By introducing a module to predict the “loss” of the unlabeled samples, it estimates sample uncertainty and selects samples with large “loss” like hard negative mining.

2.2. Active Learning for Object Detection

Despite the substantial progress of active learning, few methods are specified for active object detection, which

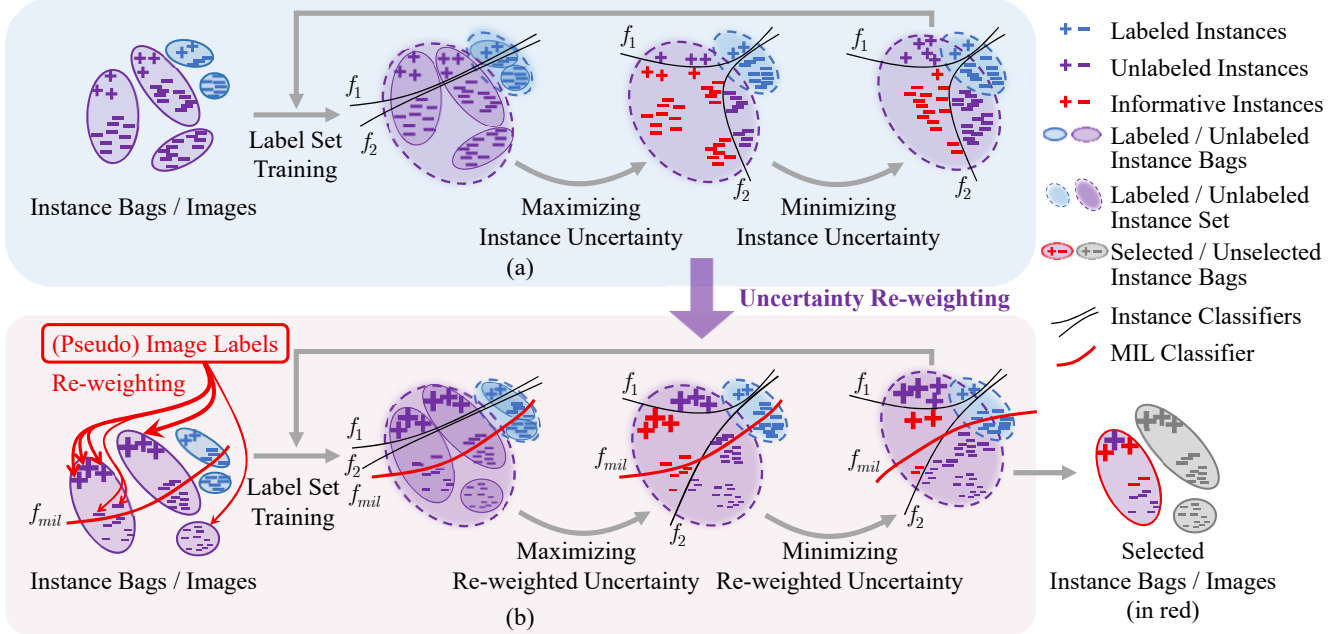


Figure 2. MI-AOD illustration. (a) Instance uncertainty learning (IUL) utilizing two adversarial classifiers. (b) Instance uncertainty re-weighting (IUR) using multiple instance learning. Bigger symbols (“+” and “-”) indicate larger weights. (Best viewed in color)

faces complex instance distributions in the same images and are more challenging than active image classification. By simply sorting the loss predictions of instances to evaluate the image uncertainty, the learning loss method [42] specified for image classification was directly applied to object detection. The image-level uncertainty can also be estimated by the uncertainty of a lot of background pixels [2]. CDAL [1] introduced spatial context to active detection and selected diverse samples according to the distances to the labeled set. Existing approaches simply used instance-/pixel-level observations to represent the image-level uncertainty. There still lacks a systematic method to learn the image uncertainty by leveraging instance-level models [44, 45].

3. The Proposed Approach

3.1. Overview

For active object detection, a small set of images \mathcal{X}_L^0 (the labeled set) with instance labels \mathcal{Y}_L^0 and a large set of images \mathcal{X}_U^0 (the unlabeled set) without labels are given. For each image, the label consists of bounding boxes (y_x^{loc}) and categories (y_x^{cls}) for objects of interest. A detection model M_0 is firstly initialized by using the labeled set $\{\mathcal{X}_L^0, \mathcal{Y}_L^0\}$. With the initialized model M_0 , active learning targets at selecting a set of images \mathcal{X}_S^0 from \mathcal{X}_U^0 to be manually labeled and merging them with \mathcal{X}_L^0 for a new labeled set \mathcal{X}_L^1 , *i.e.*, $\mathcal{X}_L^1 = \mathcal{X}_L^0 \cup \mathcal{X}_S^0$. The selected image set \mathcal{X}_S^0 should be the most informative, *i.e.*, can improve the detection performance as much as possible. Based on the updated labeled

set \mathcal{X}_L^1 , the task model is retrained and updated to M_1 . The model training and sample selection repeat some cycles until the size of labeled set reaches the annotation budget.

Considering the large number¹ of instances in each image, there are two key problems for active object detection: (1) how to evaluate the uncertainty of the unlabeled instances using the detector trained on the labeled set; (2) how to precisely estimate the image uncertainty while filtering out noisy instances. MI-AOD handles these two problems by introducing two learning modules respectively. For the first problem, MI-AOD incorporates instance uncertainty learning, with the aim of highlighting informative instances in the unlabeled set, as well as aligning the distributions of the labeled and unlabeled set, Fig. 2(a). It is motivated by the fact that most active learning methods remain simply generalizing the models trained on the labeled set to the unlabeled set. This is problematic when there is a distribution bias between the two sets [10]. For the second problem, MI-AOD introduces MIL to both the labeled and unlabeled set to estimate the image uncertainty by re-weighting the instance uncertainty. This is done by treating each image as an instance bag while re-weighting the instance uncertainty under the supervision of the image classification loss. Optimizing the image classification loss facilitates highlighting truly representative instances belonging to the same object classes while suppressing the noisy ones, Fig. 2(b).

¹For example, the RetinaNet detector [19] produces ~100k of anchors (instances) for an image.

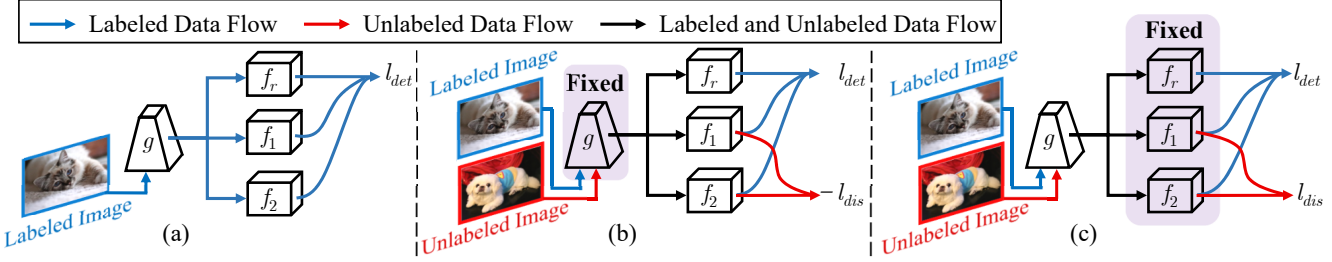


Figure 3. Network architecture for instance uncertainty learning. (a) Label set training. (b) Maximizing instance uncertainty by maximizing classifier prediction discrepancy. (c) Minimizing instance uncertainty by minimizing classifier prediction discrepancy.

3.2. Instance Uncertainty Learning

Label Set Training. Using the RetinaNet as the baseline [19], we construct a detector with two discrepant instance classifiers (f_1 and f_2) and a bounding box regressor (f_r), Fig. 3(a). We utilize the prediction discrepancy between the two instance classifiers to learn the instance uncertainty on the unlabeled set. Let g denote the feature extractor parameterized by θ_g . The discrepant classifiers are parameterized by θ_{f_1} and θ_{f_2} and the regressor by θ_{f_r} . $\Theta = \{\theta_{f_1}, \theta_{f_2}, \theta_{f_r}, \theta_g\}$ denotes the set of all parameters, where θ_{f_1} and θ_{f_2} are independently initialized.

In object detection, each image x can be represented by multiple instances $\{x_i, i = 1, \dots, N\}$ corresponding to the feature anchors on the feature map [19]. N is the number of the instances in image x . $\{y_i, i = 1, \dots, N\}$ denote the labels for the instances. Given the labeled set, a detection model is trained by optimizing the detection loss, as

$$\begin{aligned} \operatorname{argmin}_{\Theta} l_{det}(x) = \sum_i & \left(FL(\hat{y}_i^{f_1}, y_i^{cls}) + FL(\hat{y}_i^{f_2}, y_i^{cls}) \right. \\ & \left. + SmoothL1(\hat{y}_i^{f_r}, y_i^{loc}) \right), \end{aligned} \quad (1)$$

where $FL(\cdot)$ is the focal loss function for instance classification and $SmoothL1(\cdot)$ is the smooth L1 loss function for bounding box regression [19]. $\hat{y}_i^{f_1} = f_1(g(x_i))$, $\hat{y}_i^{f_2} = f_2(g(x_i))$ and $\hat{y}_i^{f_r} = f_r(g(x_i))$ denote the prediction results (classification and localization) for the instances. y_i^{cls} and y_i^{loc} denote the ground-truth class label and bounding box label, respectively.

Maximizing Instance Uncertainty. Before the labeled set can precisely represent the unlabeled set, there exists a distribution bias between the labeled and unlabeled set, especially when the labeled set is small. The informative instances are in the biased distribution area. To find them out, f_1 and f_2 are designed as the adversarial instance classifiers with larger prediction discrepancy on the instances close to the boundary, Fig. 2(a). The instance uncertainty is defined as the prediction discrepancy of f_1 and f_2 .

To find out the most informative instances, it requires to fine-tune the network and maximize the prediction discrepancy

of the adversarial classifiers, Fig. 3(b). In this procedure, θ_g is fixed so that the distributions of both the labeled and unlabeled instances are fixed. θ_{f_1} and θ_{f_2} are fine-tuned on the unlabeled set to maximize the prediction discrepancies for all instances. At the same time, it requires to preserve the detection performance on the labeled set. This is fulfilled by optimizing the following loss function, as

$$\operatorname{argmin}_{\Theta \setminus \theta_g} \mathcal{L}_{max} = \sum_{x \in \mathcal{X}_L} l_{det}(x) - \sum_{x \in \mathcal{X}_U} \lambda \cdot l_{dis}(x), \quad (2)$$

where

$$l_{dis}(x) = \sum_i |\hat{y}_i^{f_1} - \hat{y}_i^{f_2}| \quad (3)$$

denotes the prediction discrepancy loss. $\hat{y}_i^{f_1}, \hat{y}_i^{f_2} \in \mathbb{R}^{1 \times C}$ are the instance classification predictions of the two classifiers for the i -th instance in image x , where C is the number of object classes in the dataset. λ is a regularization hyper-parameter. As shown in Fig. 2(a), the informative instances with different predictions by the adversarial classifiers tend to have larger prediction discrepancy and larger uncertainty.

Minimizing Instance Uncertainty. After maximizing the prediction discrepancy, we further propose to minimize the prediction discrepancy to align the distributions of the labeled and unlabeled instances, Fig. 3(c). In this procedure, the classifier parameters θ_{f_1} and θ_{f_2} are fixed, while the parameters θ_g of the feature extractor are optimized by minimizing the prediction discrepancy loss, as

$$\operatorname{argmin}_{\theta_g} \mathcal{L}_{min} = \sum_{x \in \mathcal{X}_L} l_{det}(x) + \sum_{x \in \mathcal{X}_U} \lambda \cdot l_{dis}(x). \quad (4)$$

By minimizing the prediction discrepancy, the distribution bias between the labeled set and the unlabeled set is minimized and their features are aligned as much as possible.

In each active learning cycle, the max-min prediction discrepancy procedures repeat several times so that the instance uncertainty is learned and the instance distributions of the labeled and unlabeled set are progressively aligned. This actually defines an unsupervised learning procedure, which leverages the information (*i.e.*, prediction discrepancy) of the unlabeled set to improve the detection model.

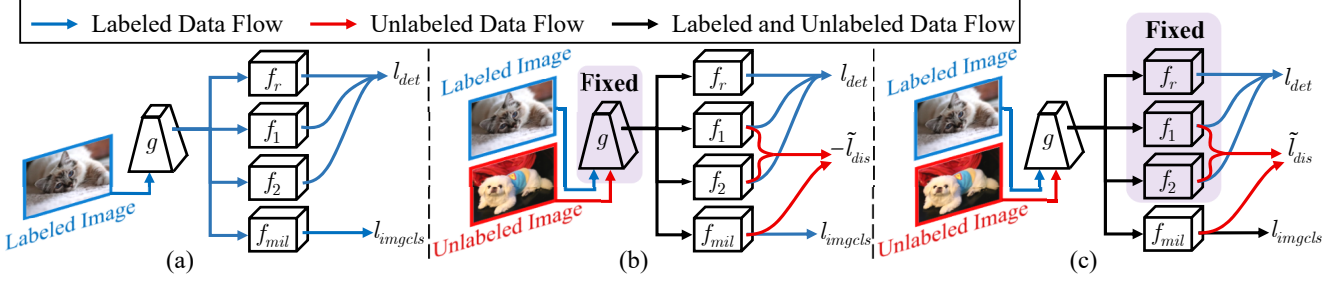


Figure 4. Network architecture for instance uncertainty re-weighting. (a) Label set training. (b) Re-weighting and maximizing instance uncertainty. (c) Re-weighting while minimizing instance uncertainty.

3.3. Instance Uncertainty Re-weighting

With instance uncertainty learning, the informative instances are highlighted. However, as there is a lot of instances ($\sim 100k$) in each image, the instance uncertainty may be not consistent with the image uncertainty. Some instances of high uncertainty are simply background noise or hard negatives for the detector. We thereby introduce an MIL procedure to bridge the gap between the instance-level and image-level uncertainty by filtering out noisy instances.

Multiple Instance Learning. MIL treats each image as an instance bag and utilizes the instance classification predictions to estimate the bag labels. In turn, it re-weights the instance uncertainty scores by minimizing the image classification loss. This actually defines an Expectation-Maximization procedure [35, 5] to re-weight instance uncertainty across bags while filtering out noisy instances.

Specifically, we add an MIL classifier f_{mil} parameterized by $\theta_{f_{mil}}$ in parallel with the instance classifiers, Fig. 4. The image classification score $\hat{y}_{i,c}^{cls}$ for multiple instances in an image is calculated as

$$\hat{y}_{i,c}^{cls} = \frac{\exp(\hat{y}_{i,c}^{f_{mil}})}{\sum_c \exp(\hat{y}_{i,c}^{f_{mil}})} \cdot \frac{\exp((\hat{y}_{i,c}^{f_1} + \hat{y}_{i,c}^{f_2})/2)}{\sum_i \exp((\hat{y}_{i,c}^{f_1} + \hat{y}_{i,c}^{f_2})/2)}, \quad (5)$$

where $\hat{y}^{f_{mil}} = f_{mil}(g(x))$ is an $N \times C$ score matrix, and $\hat{y}_{i,c}^{f_{mil}}$ is the element in $\hat{y}^{f_{mil}}$ indicating the score of the i -th instance for class c . According to Eq. (5), the image classification score $\hat{y}_{i,c}^{cls}$ is large only when x_i belongs to class c (the first term in Eq. (5)) and its instance classification scores $\hat{y}_{i,c}^{f_1}$ and $\hat{y}_{i,c}^{f_2}$ are significantly larger than those of others (the second term in Eq. (5)).

Considering that the image classification scores of the instances from other classes/backgrounds are small, the image classification loss l_{imgcls} is defined as

$$l_{imgcls}(x) = - \sum_c \left(y_c^{cls} \log \sum_i \hat{y}_{i,c}^{cls} + (1 - y_c^{cls}) \log(1 - \sum_i \hat{y}_{i,c}^{cls}) \right), \quad (6)$$

where $y_c^{cls} \in \{0, 1\}$ denotes the image class label, which can be directly obtained from the instance class label y_i^{cls} in the labeled set. Optimizing Eq. (6) drives the MIL classifier to activate instances with large MIL score ($\hat{y}_{i,c}^{f_{mil}}$) and large classification outputs ($\hat{y}_{i,c}^{f_1} + \hat{y}_{i,c}^{f_2}$). The instances with small MIL scores will be suppressed as background. The image classification loss is firstly applied in the label set training to get the initial model, and then used to re-weight the instance uncertainty in the unlabeled set.

Uncertainty Re-weighting. To ensure that the instance uncertainty is consistent with the image uncertainty, we assemble the image classification scores for all classes to a score vector w_i and re-weight the instance uncertainty as

$$\tilde{l}_{dis}(x) = \sum_i |w_i \cdot (\hat{y}_i^{f_1} - \hat{y}_i^{f_2})|, \quad (7)$$

where $w_i = \hat{y}_i^{cls}$. We then update Eq. (2) to

$$\operatorname{argmin}_{\tilde{\Theta} \setminus \theta_g} \tilde{\mathcal{L}}_{max} = \sum_{x \in \mathcal{X}_L} \left(l_{det}(x) + l_{imgcls}(x) \right) - \sum_{x \in \mathcal{X}_U} \lambda \cdot \tilde{l}_{dis}(x), \quad (8)$$

where $\tilde{\Theta} = \Theta \cup \{\theta_{f_{mil}}\}$. By optimizing Eq. (8), the discrepancies of instances with large image classification scores are preferentially estimated, while those with small classification scores are suppressed. Similarly, Eq. (4) is updated to

$$\begin{aligned} \operatorname{argmin}_{\theta_g, \theta_{f_{mil}}} \tilde{\mathcal{L}}_{min} &= \sum_{x \in \mathcal{X}_L} \left(l_{det}(x) + l_{imgcls}(x) \right) \\ &+ \sum_{x \in \mathcal{X}_U} \left(\lambda \cdot \tilde{l}_{dis}(x) + l_{imgcls}(x) \right). \end{aligned} \quad (9)$$

In Eq. (9), the image classification loss is applied to the unlabeled set, where the pseudo image labels are estimated using the outputs of the instance classifiers, as

$$y_c^{pseudo} = \mathbb{1} \left(\max_i \left(\frac{\hat{y}_{i,c}^{f_1} + \hat{y}_{i,c}^{f_2}}{2} \right), 0.5 \right), \quad (10)$$

where $\mathbb{1}(a, b)$ is a binarization function. When $a > b$, it returns 1; otherwise 0. Eq. (10) is defined based on that instance classifiers can find true instances but are easy to

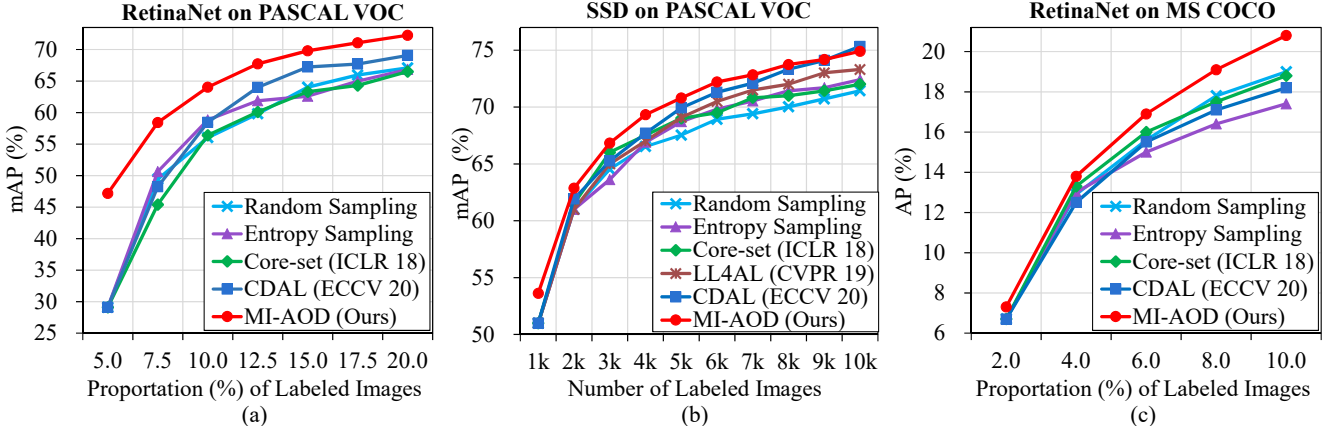


Figure 5. Performance comparison of active object detection methods. (a) On PASCAL VOC using RetinaNet backbone. (b) On PASCAL VOC using SSD backbone. (c) On MS COCO using RetinaNet backbone.

be confused by complex backgrounds. We use the maximum instance score to predict pseudo image labels and leverage MIL to reduce background interference. According to Eqs. (5) and (6), the image classification loss ensures the highlighted instances are representative of the image, *i.e.*, minimizing the image classification loss so that the gap between the instance uncertainty and image uncertainty is minimized. By iteratively optimizing Eqs. (8) and (9), informative object instances with the same class are statistically highlighted, while the background instances are suppressed during the instance uncertainty learning procedure.

3.4. Informative Image Selection

In each learning cycle, after instance uncertainty learning (IUL) and instance uncertainty re-weighting (IUR), we select the most informative images from the unlabeled set by observing the top- k instance uncertainty defined in Eq. (3) for each image, where k is a hyper-parameter. This is based on the fact that the noisy instances have been suppressed and the instance uncertainty becomes consistent with the image uncertainty. The selected images are merged into the labeled set for the next learning cycle.

4. Experiments

4.1. Experimental Settings

Datasets. The *trainval* sets of PASCAL VOC 2007 and 2012 datasets which contain 5011 and 11540 images are used for training. The VOC 2007 *test* set is used to evaluate mean average precision (mAP). The MS COCO dataset contains 80 object categories with challenging aspects including dense objects and small objects with occlusion. We use the *train* set with 117k images for active learning and the *val* set with 5k images for evaluating AP.

Active Learning Settings. We use the RetinaNet [19] with ResNet-50 and SSD [23] with VGG-16 as the base de-

tector. For RetinaNet, MI-AOD uses 5.0% of randomly selected images from the training set to initialize the labeled set on PASCAL VOC. In each active learning cycle, it selects 2.5% images from the rest unlabeled set until the labeled images reach 20.0% of the training set. For the large-scale MS COCO, MI-AOD uses only 2.0% of randomly selected images from the training set to initialize the labeled set. It then selects 2.0% images from the rest of the unlabeled set in each cycle until reaching 10.0% of the training set. In each cycle, the model is trained for 26 epochs with the mini-batch size 2 and the learning rate 0.001. After 20 epochs, the learning rate decreases to 0.0001. The momentum and the weight decay are set to 0.9 and 0.0005 respectively. For SSD, we follow the settings in [42] and [1], where 1k images in PASCAL VOC dataset are selected to initialize the labeled set and 1k images are selected in each cycle. The learning rate is 0.001 for the first 240 epochs and reduced to 0.0001 for the last 60 epochs. The mini-batch size is set to 32 which is required by LL4AL [42].

We compare MI-AOD with random sampling, entropy sampling, Core-set [30], LL4AL [42] and CDAL [1]. For entropy sampling, we use the averaged instance entropy as the image uncertainty. We repeat all experiments for 5 times and use the mean performance. MI-AOD and other methods share the same random seed and initialization for a fair comparison. λ defined in Eqs. (2), (4), (8) and (9) is set to 0.5 and k mentioned in Sec. 3.4 is set to 10k.

4.2. Performance

PASCAL VOC. In Fig. 5, we report the performance of MI-AOD and compare it with state-of-the-art methods on a TITAN V GPU. Using either the RetinaNet [19] or SSD [22] detector, MI-AOD outperforms state-of-the-art methods with large margins. Particularly, it respectively outperforms state-of-the-art methods by 18.08%, 7.78%, and 5.19% when using 5.0%, 7.5%, and 10.0% samples.

Training		Sample Selection			mAP (%) on Proportion (%) of Labeled Images								
IUL	IUR	Rand.	Max Unc.	Mean Unc.	5.0	7.5	10.0	12.5	15.0	17.5	20.0	100.0	
		✓			28.31	49.42	56.03	59.81	64.02	65.95	67.09		
✓		✓			30.09	49.17	55.64	60.93	64.10	65.77	67.20	77.28	
✓			✓		30.09	49.79	58.94	63.11	65.61	67.84	69.01		
✓				✓	30.09	49.74	60.60	64.29	67.13	68.76	70.06		
		✓	✓		47.18	57.12	60.68	63.72	66.10	67.59	68.48		
			✓		47.18	57.58	61.74	64.58	66.98	68.79	70.33	78.37	
		✓		✓	47.18	58.03	63.98	66.58	69.57	70.96	72.03		

Table 1. Module ablation on PASCAL VOC. The first line shows the result of the baseline method with random image selection. “Max Unc.” and “Mean Unc.” respectively denote that the image uncertainty is represented by the maximum and averaged instance uncertainty.

Training	mAP (%) on Proportion (%) of Labeled Img.				
IUL	2.0	4.0	6.0	8.0	10.0
	51.01	61.48	69.14	75.14	79.77
✓	58.07	67.75	74.91	78.88	80.96

Table 2. The effect of IUL for active image classification. Experiments are conducted on CIFAR-10 using the ResNet-18 backbone while the images are randomly selected in all cycles.

With 20.0% samples, MI-AOD achieves 72.27% detection mAP, which significantly outperforms CDAL by 3.20%. The improvements validate that MI-AOD can precisely learn instance uncertainty while selecting informative images. When using the SSD detector, MI-AOD outperforms state-of-the-art methods in almost all cycles, demonstrating the general applicability of MI-AOD to object detectors.

MS COCO. MS COCO is a challenging dataset for more categories, denser objects, and larger scale variation, where MI-AOD also outperforms the compared methods, Fig. 5. Particularly, it respectively outperforms Core-set and CDAL by 0.6%, 0.5%, and 2.0%, and 0.6%, 1.3%, and 2.6% when using 2.0%, 4.0%, and 10.0% labeled images.

4.3. Ablation Study

IUL. As shown in Tab. 1, with IUL, the detection performance is improved up to 70.06% in the last cycle, which outperforms the Random method by 2.97% (70.06% *vs.* 67.09%). In Tab. 2, IUL also significantly improves the image classification performance with active learning on CIFAR-10. Particularly when using 2.0% samples, it improves the classification performance by 7.06% (58.07% *vs.* 51.01%), demonstrating the effectiveness of the discrepancy learning module for instance uncertainty estimation.

IUR. In Tab. 1, IUL achieves comparable performance

w_i	Set	mAP (%) on Proportion (%) of Labeled Img.						
		5.0	7.5	10.0	12.5	15.0	17.5	20.0
1	\emptyset	30.09	49.17	55.64	60.93	64.10	65.77	67.20
$\hat{y}_i^{f_1}$	\emptyset	31.67	50.67	55.93	60.78	64.17	66.22	67.30
1	\mathcal{X}_L	42.52	54.08	57.18	63.43	65.04	66.74	68.32
\hat{y}_i^{cls}	\mathcal{X}	47.18	57.12	60.68	63.72	66.10	67.59	68.48

Table 3. Ablation study on IUR. “ w_i ” is the w_i in Eq. (7). “Set” denotes the sample set for IUR. \mathcal{X} and \mathcal{X}_L denote the whole sample set and the labeled set, respectively.

with the method using the random image selection strategy in the early cycles. This is because there are significant noisy instances that make the instance uncertainty inconsistent with image uncertainty. After using IUR to re-weight instance uncertainty, the performance at early cycles is improved by 5.04%~17.09% in the first three cycles (row 4 *vs.* row 1 in Tab. 3). In the last cycle, the performance is improved by 1.28% (68.48% *vs.* 67.20%) in comparison with IUL and 1.39% in comparison with the Random method (68.48% *vs.* 67.09%). As shown in Tab. 3, image classification score \hat{y}_i^{cls} is the best re-weighting metric (row 4 *vs.* others). Interestingly, when using 100.0% images for training, the detector with IUR outperforms the detector without IUR by 1.09% (78.37% *vs.* 77.28%). These results clearly verify that the IUR module can suppress the interfering instances while highlighting more representative ones, which can indicate informative images for detector training.

Hyper-parameters and Time Cost. The effects of the regularization factor λ defined in Eqs. (2), (4), (8) and (9) and the valid instance number k in each image for selection are shown in Tab. 4. One can see that we have the best performance when λ is set to 0.5 and k is set to 10k (for ~100k instances/anchors in each image). Tab. 5 shows that

λ	k	mAP (%) on Proportion (%) of Labeled Imgs.						
		5.0	7.5	10.0	12.5	15.0	17.5	20.0
2	10k	47.18	56.94	64.44	67.70	69.58	70.67	72.12
1	10k	47.18	57.30	64.93	67.40	69.63	70.53	71.62
0.5	10k	47.18	58.41	64.02	67.72	69.79	71.07	72.27
0.2	10k	47.18	58.02	64.44	67.67	69.42	70.98	72.06
0.5	N	47.18	58.03	63.98	66.58	69.57	70.96	72.03
0.5	10k	47.18	58.41	64.02	67.72	69.79	71.07	72.27
0.5	100	47.18	58.74	63.62	67.03	68.63	70.26	71.47
0.5	1	47.18	57.58	61.74	64.58	66.98	68.79	70.33

Table 4. Performance under different hyper-parameters.

Method	Time (h) on Proportion (%) of Labeled Imgs.						
	5.0	7.5	10.0	12.5	15.0	17.5	20.0
Random	0.77	1.12	1.45	1.78	2.12	2.45	2.78
CDAL [1]	1.18	1.50	1.87	2.19	2.68	2.83	2.82
MI-AOD	1.03	1.42	1.78	2.18	2.55	2.93	3.12

Table 5. Comparison of time cost on PASCAL VOC.

MI-AOD costs less time at early cycles and slightly more time at later cycles than CDAL.

4.4. Model Analysis

Visualization Analysis. In Fig. 6, we visualize the learned and re-weighted uncertainty and image classification scores of instances. The heatmaps are calculated by summarizing the uncertainty scores of all instances. With only IUL, there exist interference instances from the background (row 1) or around the true positive instance (row 2), and the results tend to miss the true positive instances (row 3) or instance parts (row 4). MIL can assign high image classification scores to the instances of interesting while suppressing backgrounds. As a result, IUR leverages the image classification scores to re-weight instances towards accurate instance uncertainty prediction.

Statistical Analysis. In Fig. 7, we calculate the number of true positive instances selected in each active learning cycle. It can be seen that MI-AOD hits significantly more true positives in all learning cycles. This shows that the proposed MI-AOD approach can better activate true positive objects while filtering out interfering instances, which facilitates selecting informative images for detector training.

5. Conclusion

We proposed Multiple Instance Active Object Detection (MI-AOD) to select informative images for detector training

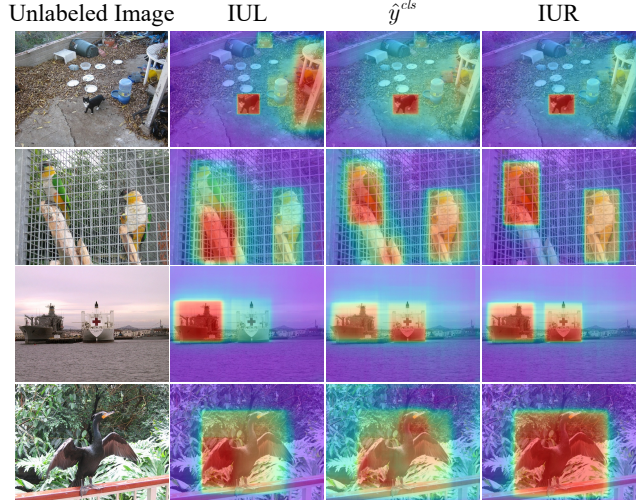


Figure 6. Visualization of learned and re-weighted instance uncertainty and image classification score. (Best viewed in color)

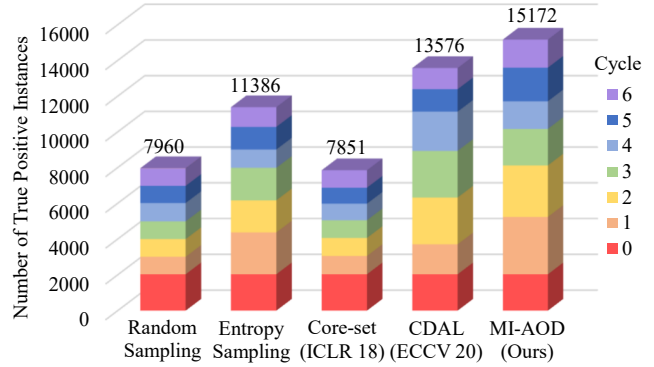


Figure 7. The number of true positive instances selected in each active learning cycle on PASCAL VOC using RetinaNet backbone.

by observing instance uncertainty. MI-AOD incorporates a discrepancy learning module, which leverages adversarial instance classifiers to learn the uncertainty of unlabeled instances. MI-AOD treats the unlabeled images as instance bags and estimates the image uncertainty by re-weighting instances in a multiple instance learning (MIL) fashion. Iterative instance uncertainty learning and re-weighting facilitate suppressing noisy instances, towards selecting informative images for detector training. Experiments on large-scale datasets have validated the superiority of MI-AOD, in striking contrast with state-of-the-art methods. MI-AOD sets a solid baseline for active object detection.

Acknowledgement. This work was supported by Natural Science Foundation of China (NSFC) under Grant 62006216, 61836012 and 61771447, the Strategic Priority Research Program of Chinese Academy of Sciences under Grant No. XDA27000000 and CAAI-Huawei MindSpore Open Fund.

References

- [1] Sharat Agarwal, Himanshu Arora, Saket Anand, and Chetan Arora. Contextual diversity for active learning. In *ECCV*, pages 137–153, 2020. [2](#), [3](#), [6](#), [8](#)
- [2] Hamed Habibi Aghdam, Abel Gonzalez-Garcia, Antonio M. López, and Joost van de Weijer. Active learning for deep detection neural networks. In *ICCV*, pages 3671–3679, 2019. [2](#), [3](#)
- [3] Oisin Mac Aodha, Neill D. F. Campbell, Jan Kautz, and Gabriel J. Brostow. Hierarchical subquery evaluation for active learning on a graph. In *CVPR*, pages 564–571, 2014. [2](#)
- [4] William H. Beluch, Tim Genewein, Andreas Nürnberger, and Jan M. Köhler. The power of ensembles for active learning in image classification. In *CVPR*, pages 9368–9377, 2018. [2](#)
- [5] Hakan Bilen and Andrea Vedaldi. Weakly supervised deep detection networks. In *CVPR*, pages 2846–2854, 2016. [5](#)
- [6] Marc-Andre Carbonneau, Eric Granger, and Ghyslain Gagnon. Bag-level aggregation for multiple-instance active learning in instance classification problems. *IEEE TNNLS*, 30(5):1441–1451, 2019. [2](#)
- [7] Ehsan Elhamifar, Guillermo Sapiro, Allen Y. Yang, and S. Shankar Sastry. A convex optimization framework for active learning. In *ICCV*, pages 209–216, 2013. [2](#)
- [8] Alexander Freytag, Erik Rodner, and Joachim Denzler. Selecting influential examples: Active learning with expected model output changes. In *ECCV*, pages 562–577, 2014. [2](#)
- [9] Yarin Gal, Riashat Islam, and Zoubin Ghahramani. Deep bayesian active learning with image data. In *ICML*, pages 1183–1192, 2017. [2](#)
- [10] Denis A. Gudovskiy, Alec Hodgkinson, Takuya Yamaguchi, and Sotaro Tsukizawa. Deep active learning for biased datasets via fisher kernel self-supervision. In *CVPR*, pages 9038–9046, 2020. [3](#)
- [11] Yuhong Guo. Active instance sampling via matrix partition. In *NeurIPS*, pages 802–810, 2010. [2](#)
- [12] Mahmudul Hasan and Amit K. Roy-Chowdhury. Context aware active learning of activity recognition models. In *ICCV*, pages 4543–4551, 2015. [2](#)
- [13] Sheng-Jun Huang, Nengneng Gao, and Songcan Chen. Multi-instance multi-label active learning. In *IJCAI*, pages 1886–1892, 2017. [2](#)
- [14] Ajay J. Joshi, Fatih Porikli, and Nikolaos Papanikopoulos. Multi-class active learning for image classification. In *CVPR*, pages 2372–2379, 2009. [2](#)
- [15] Christoph Käding, Erik Rodner, Alexander Freytag, and Joachim Denzler. Active and continuous exploration with deep neural networks and expected model output changes. *arXiv preprint arXiv:1612.06129*, 2016. [2](#)
- [16] David D. Lewis and Jason Catlett. Heterogeneous uncertainty sampling for supervised learning. In *Machine Learning*, pages 148–156, 1994. [2](#)
- [17] David D. Lewis and William A. Gale. A sequential algorithm for training text classifiers. In *SIGIR*, pages 3–12, 1994. [2](#)
- [18] Liang Lin, Keze Wang, Deyu Meng, Wangmeng Zuo, and Lei Zhang. Active self-paced learning for cost-effective and progressive face identification. *IEEE TPAMI*, 40(1):7–19, 2018. [2](#)
- [19] Tsung-Yi Lin, Priya Goyal, Ross B. Girshick, Kaiming He, and Piotr Dollár. Focal loss for dense object detection. *IEEE TPAMI*, 42(2):318–327, 2020. [3](#), [4](#), [6](#)
- [20] Binghao Liu, Yao Ding, Jianbin Jiao, Ji Xiangyang, and Qixiang Ye. Anti-aliasing semantic reconstruction for few-shot semantic segmentation. In *CVPR*, 2021. [1](#)
- [21] Binghao Liu, Jianbin Jiao, and Qixiang Ye. Harmonic feature activation for few-shot semantic segmentation. *IEEE TIP*, pages 3142–3153, 2021. [1](#)
- [22] Wei Liu, Dragomir Anguelov, Dumitru Erhan, Christian Szegedy, Scott Reed, Cheng-Yang Fu, and Alexander C Berg. Ssd: Single shot multibox detector. In *ECCV*, pages 21–37, 2016. [6](#)
- [23] Wei Liu, Dragomir Anguelov, Dumitru Erhan, Christian Szegedy, Scott E. Reed, Cheng-Yang Fu, and Alexander C. Berg. SSD: single shot multibox detector. In *ECCV*, pages 21–37, 2016. [6](#)
- [24] Zhao-Yang Liu and Sheng-Jun Huang. Active sampling for open-set classification without initial annotation. In *AAAI*, pages 4416–4423, 2019. [2](#)
- [25] Zhao-Yang Liu, Shao-Yuan Li, Songcan Chen, Yao Hu, and Sheng-Jun Huang. Uncertainty aware graph gaussian process for semi-supervised learning. In *AAAI*, pages 4957–4964, 2020. [2](#)
- [26] Wenjie Luo, Alexander G. Schwing, and Raquel Urtasun. Latent structured active learning. In *NeurIPS*, pages 728–736, 2013. [2](#)
- [27] Hieu Tat Nguyen and Arnold W. M. Smeulders. Active learning using pre-clustering. In *ICML*, 2004. [2](#)
- [28] Dan Roth and Kevin Small. Margin-based active learning for structured output spaces. In *ECML*, pages 413–424, 2006. [2](#)
- [29] Nicholas Roy and Andrew McCallum. Toward optimal active learning through sampling estimation of error reduction. In *ICML*, pages 441–448, 2001. [2](#)
- [30] Ozan Sener and Silvio Savarese. Active learning for convolutional neural networks: A core-set approach. In *ICLR*, 2018. [2](#), [6](#)
- [31] Burr Settles. *Active Learning*. Synthesis Lectures on Artificial Intelligence and Machine Learning. 2012. [2](#)
- [32] Burr Settles and Mark Craven. An analysis of active learning strategies for sequence labeling tasks. In *EMNLP*, pages 1070–1079, 2008. [2](#)
- [33] Burr Settles, Mark Craven, and Soumya Ray. Multiple-instance active learning. In *NeurIPS*, pages 1289–1296, 2007. [2](#)
- [34] Samarth Sinha, Sayna Ebrahimi, and Trevor Darrell. Variational adversarial active learning. In *ICCV*, pages 5971–5980, 2019. [2](#)
- [35] Andrews Stuart, Tsochantaridis Ioannis, and Hofmann Thomas. Support vector machines for multiple-instance learning. In *NeurIPS*, pages 561–568, 2002. [5](#)
- [36] Ying-Peng Tang and Sheng-Jun Huang. Self-paced active learning: Query the right thing at the right time. In *AAAI*, pages 5117–5124, 2019. [2](#)

- [37] Fang Wan, Chang Liu, Wei Ke, Xiangyang Ji, Jianbin Jiao, and Qixiang Ye. C-mil: Continuation multiple instance learning for weakly supervised object detection. In *CVPR*, pages 2199–2208, 2019. [2](#)
- [38] Fang Wan, Pengxu Wei, Zhenjun Han, Jianbin Jiao, and Qixiang Ye. Min-entropy latent model for weakly supervised object detection. *IEEE TPAMI*, 41(10):2395–2409, 2019. [2](#)
- [39] Keze Wang, Dongyu Zhang, Ya Li, Ruimao Zhang, and Liang Lin. Cost-effective active learning for deep image classification. *IEEE TCSVT*, 27(12):2591–2600, 2017. [2](#)
- [40] Ran Wang, Xi-Zhao Wang, Sam Kwong, and Chen Xu. Incorporating diversity and informativeness in multiple-instance active learning. *IEEE TFS*, 25(6):1460–1475, 2017. [2](#)
- [41] Yi Yang, Zhigang Ma, Feiping Nie, Xiaojun Chang, and Alexander G. Hauptmann. Multi-class active learning by uncertainty sampling with diversity maximization. *IJCV*, 113(2):113–127, 2015. [2](#)
- [42] Donggeun Yoo and In So Kweon. Learning loss for active learning. In *CVPR*, pages 93–102, 2019. [2](#), [3](#), [6](#)
- [43] Beichen Zhang, Liang Li, Shijie Yang, Shuhui Wang, Zheng-Jun Zha, and Qingming Huang. State-relabeling adversarial active learning. In *CVPR*, pages 8753–8762, 2020. [2](#)
- [44] Xiaosong Zhang, Fang Wan, Chang Liu, Rongrong Ji, and Qixiang Ye. Freeanchor: Learning to match anchors for visual object detection. In *NeurIPS*, pages 147–155, 2019. [3](#)
- [45] Xiaosong Zhang, Fang Wan, Chang Liu, Xiangyang Ji, and Qixiang Ye. Learning to match anchors for visual object detection. *IEEE TPAMI*, pages 1–14, 2021. [3](#)